



HAL
open science

AsiDNA Is a Radiosensitizer with no Added Toxicity in Medulloblastoma Pediatric Models

Sofia Ferreira, Chloe Foray, Alberto Gatto, Magalie Larcher, Sophie Heinrich, Mihaela Lupu, Joel Mispelter, François Boussin, Celio Pouponnot, Marie Dutreix

► **To cite this version:**

Sofia Ferreira, Chloe Foray, Alberto Gatto, Magalie Larcher, Sophie Heinrich, et al.. AsiDNA Is a Radiosensitizer with no Added Toxicity in Medulloblastoma Pediatric Models. *Clinical Cancer Research*, 2020, 26 (21), pp.5735-5746. 10.1158/1078-0432.CCR-20-1729 . hal-03043490

HAL Id: hal-03043490

<https://hal.science/hal-03043490>

Submitted on 18 Dec 2020

HAL is a multi-disciplinary open access archive for the deposit and dissemination of scientific research documents, whether they are published or not. The documents may come from teaching and research institutions in France or abroad, or from public or private research centers.

L'archive ouverte pluridisciplinaire **HAL**, est destinée au dépôt et à la diffusion de documents scientifiques de niveau recherche, publiés ou non, émanant des établissements d'enseignement et de recherche français ou étrangers, des laboratoires publics ou privés.

AsiDNA is a radiosensitizer with no added toxicity in medulloblastoma pediatric models

Sofia Ferreira^{1,2}, Chloe Foray^{1,2}, Alberto Gatto^{3,4} Magalie Larcher^{1,2}, Sophie Heinrich^{1,2}, Mihaela Lupu^{5,6}, Joel Mispelter^{5,6}, Francois D. Boussin⁷, Celio Pouponnot^{1,2}, Marie Dutreix^{1,2} *

¹ Institut Curie, PSL Research University, CNRS UMR 3347, INSERM U1021, F-91405 Orsay, France.

² Institut Curie, Université Paris-Sud, Université Paris-Saclay, CNRS UMR 3347, INSERM U1021, F-91405 Orsay, France.

³ Institut Curie, Paris Sciences et Lettres Research University, Centre National de la Recherche Scientifique, UMR3664, Equipe Labellisée Ligue contre le Cancer, Paris, France.

⁴ Sorbonne Universités, Université Pierre et Marie Curie Paris 06, Centre National de la Recherche Scientifique, UMR3664, Paris, France

⁵ Institut Curie, Research Center, PSL Research University, CNRS UMR 9187, INSERM U 1196, F-91405 Orsay, France.

⁶ Institut Curie, Université Paris-Sud, Université Paris-Saclay, CNRS UMR 9187, INSERM U1196, F-91405 Orsay, France

⁷ UMR Stabilité Génétique Cellules Souches et Radiations, Inserm, Université de Paris, Université Paris-Saclay, CEA, 18 route du Panorama 92265 Fontenay-aux Roses, France.

Running title: AsiDNA to radiosensitize medulloblastoma

* *To whom correspondence should be addressed: Marie Dutreix, Institut Curie UMR3347. Université Paris-Sud, Building 112. 15, rue Georges Clémenceau – F-91405 Orsay, France. Tel: +33 1 69 86 71 86; Fax: +33 1 69 86 31 41; Email: marie.dutreix@curie.fr.*

Conflict of interest: M. D. is a consultant for Onxeo and is the scientific founder of DNA therapeutics.

Statement of translational relevance (120 – 150 words)

Medulloblastoma (MB) is an important cause of mortality and morbidity in pediatric oncology. Here we propose the use the brain-penetrant DNA repair inhibitor AsiDNA, to enhance radiotherapy efficacy in MB. Our work provides robust evidence on the well-tolerated radiosensitizing properties of AsiDNA and how it could help address a significant unmet clinical need in MB care by improving clinical outcomes in high-risk subsets and allowing radiation de-escalation in standard-risk to mitigate the dose-dependent adverse effects. Robustness of protocols used throughout this study could help translate the therapeutic benefits of AsiDNA into other pediatric cancer models. The combination of AsiDNA with the conventionally used treatment agent, such as radiotherapy, brings this study closer to the reality of clinic practice. Potential for clinical translation exists as AsiDNA has already been tested in clinical trials, showing to be well tolerated and to be safe in combination to radiotherapy.

Abstract (<250 words)

Purpose: Medulloblastoma (MB) is an important cause of mortality and morbidity in pediatric oncology. Here we investigated whether the DNA repair inhibitor AsiDNA could help address a significant unmet clinical need in MB care, by improving radiotherapy efficacy without increasing radiation-associated toxicity.

Experimental design: To evaluate the brain permeability to AsiDNA upon systemic delivery, we injected intraperitoneally a fluorescent form of AsiDNA in models harboring brain tumors and in development. Studies evaluated toxicity associated to combination of AsiDNA with radiation in the treatment of young developing animals at subacute, related to growth and development, and chronic levels, related to brain organization and cognitive skills. Efficacy of the combination of AsiDNA with radiation was tested in two different preclinical xenografted models of high-risk MB, and in a panel of MB cell lines from different molecular subgroups and *TP53* status. Role of *TP53* on the AsiDNA-mediated radiosensitization was analyzed by RNA-Seq, DNA repair recruitment and cell death assays.

Results: Capable of penetrating young brain tissues, AsiDNA showed no added toxicity to radiation. Combination of AsiDNA with radiotherapy improved the survival of animal models more efficiently than increasing radiation doses. MB radiosensitization by AsiDNA was not restricted to a specific molecular group or status of *TP53*. Molecular mechanisms of AsiDNA, previously observed in adult malignancies, are conserved in pediatric models and resemble dose increase when combined with irradiation.

Conclusion: Our results suggest that AsiDNA is an attractive candidate to improve radiation therapy in MB, with no indication of additional toxicity in developing brain tissues.

Introduction

Medulloblastoma (MB), an embryonal tumor of the cerebellum, is the most common form of childhood brain malignancy (1). MB comprises four biologically distinct groups: WNT (Wingless), SHH (Sonic Hedgehog), Group 3 and Group 4 (2). Although management is adapted to risk, prognosis and clinical outcome within groups can vary greatly (3). Standard management includes surgery, craniospinal irradiation (CSI) and chemotherapy (4, 5), and achieves cure in approximately 75% of cases (1). Introduction of CSI in MB management was pivotal, resulting in the first reports of MB survivors (6). Notwithstanding, CSI is accountable for the widespread adverse effects in MB patients (7, 8). MB survivors often experience irreversible and disabling adverse effects in their psychological, endocrine and neurocognitive functioning (9-12). Despite aggressive and highly toxic regimens, current protocols still fail to treat high-risk subsets of the disease. MB remains an important cause of pediatric morbidity and mortality (1, 13). It is crucial to reduce treatment-related toxicity while maintaining or improving cure rates in MB care.

In our lab, we developed a pioneering family of DNA repair inhibitors, Dbait, to enhance the efficacy of genotoxic agents. Dbait molecules are composed of short double-stranded oligonucleotides, mimicking DNA double-strand breaks (DSBs) (Appendix Figure S1). Upon uptake, cells perceive Dbait as damage and trigger an aberrant activation of the DNA damage signaling pathways (14). Cellular Dbait activity is characterized by a pan-nuclear phosphorylation of H2AX (γ H2AX) and sustained high-levels of poly (ADP-ribose), respectively mediated by DNA-PK and PARP (15, 16). This aberrant activation of the DNA damage signaling pathways “blinds” cells to real chromosomal damage created by genotoxic agents and fails to signal it to downstream DNA repair factors. Dbait-treated cells do not form DNA damage foci after radiation, significantly hampering the recruitment and activity of the repair proteins (14). As a result, both main DSBs repair pathways, homologous recombination and non-homologous end joining, are inhibited. Rather than targeting a single enzyme, Dbait deregulate major pathways involved in the repair of DSBs. This broad mechanism of action makes it an effective radio- and chemo-sensitizer in a wide range of malignancies (17-26) including brain tumors, such as glioblastoma (27, 28). Preclinical studies using Dbait or its clinical form AsiDNA did not report additional toxicity of these drugs alone or in association with genotoxic agents. Moreover, recent results from the DRIIM Phase I/II clinical trial

demonstrated that local AsiDNA administration improved radiation response of melanoma skin metastases, without additional skin toxicity (29).

The sensitizing properties of AsiDNA have been extensively studied in adult cancers. However, these properties have never been tested in young models still in development or in pediatric tumor models. Therefore, we evaluated for the first time whether AsiDNA could be a good candidate to improve treatment outcomes in a pediatric cancer model as MB. Because mutations in *TP53* are rare in pediatric cancers, being reported in only 10% of sporadic MBs at diagnosis (30), we assessed the impact of p53 on the AsiDNA-sensitizing properties. This study focused in particular on high-risk Group 3, the most refractory group. Here, we offer a comprehensive assessment on efficacy and toxicity of the combinatorial protocols of AsiDNA to radiation, while considering the young age of the patients and the anatomical challenges of the tumor.

Material and methods

In vitro studies

Cell culture, constructs and transfection. MB cell lines HDMB03 (31), HDMB03-*luc*, ONS76 (Health Science Research Resources Bank), DAOY (ATCC) and UW228.1 (32) were cultured as described in (33). Glioma cell line U87-*luc* was cultured as described in (34). Absence of *Mycoplasma sp.* contamination was determined in-house using LookOut® Mycoplasma PCR (Sigma-Aldrich). Cell lines constructs and transfection are described in Appendix Supplementary Methods.

In vitro treatments. AsiDNA molecules were added directly into culture medium 15 hours before radiation treatments. Cells irradiation was performed using GSR D1 (GSM) ¹³⁷Cs unit irradiator with a dose rate of 0.8 to 1.1 Gy/minute.

Trypan blue cell viability assay. Cytotoxicity was measured by relative survival and cell death quantification. Cells were treated with 4.8 and 15.9 μM of AsiDNA and irradiated with doses of 0, 2 or 6 Gy. Both cells in suspension and attached were harvested 7 days after AsiDNA treatments, stained with 0.4 % trypan blue (Sigma Aldrich) and counted with LUNA cell automated counter (Logos Biosystems). D₅₀ was calculated using a linear regression model.

Repair factors recruitment assay. HDMB03 cells were treated with 7 μM of AsiDNA and irradiated with 6 Gy. Fixation, preparation for immunofluorescence (IF) and analysis were performed as described in (19), 2 hour after radiation. One nucleus in non-treated (NT) conditions was disregarded from analysis of BRCA1 foci due to a high number of foci (#152). Antibodies used: 53BP1 (CST, 4937, 1:100), BRCA1 (SCBT, sc-6954, 1:100) and γH2AX (Millipore, 05-636, 1:500).

Western Blotting and antibodies. Proteins extracts and signal revelation were obtained as described in (35). Membranes were hybridized overnight at 4°C with anti-p53 (CST, #9282, 1:1 000); anti-p21 (SCBT, sc-6246, 1:500) and anti-β-actin (Sigma-Aldrich, a-1978, 1:5 000).

RNA extraction. Cells were treated with 7 μM of AsiDNA and irradiated with 1.8 or 6 Gy. Total RNA was harvested using RNAeasy kit (QIAGEN) 24 hours after radiation treatments. RNA-Seq data analysis are described in Appendix Supplementary Methods.

Annexin-V/propidium iodide assay. Cells were treated with 7 μM of AsiDNA and irradiated with 6 Gy. Both cells in suspension and attached were harvested for analyses 48 hour after radiation, suspended in 1x binding buffer in the presence of 1:500 of Annexin V-FITC (abcam, ab14085) and 1:500 of propidium iodide (50 $\mu\text{g/ml}$) at room temperature prior to flow cytometry analysis.

Micronuclei assay. Cells were treated with 7 μM of AsiDNA and irradiated with 1.8 Gy. Micronuclei staining, acquisition and analysis were performed 72 hours after radiation treatments, as described in (36).

In Vivo animal studies

All in vivo experiments were carried out in strict accordance with institutional, national and European animal welfare regulations and were approved by the Local Ethical Review Board of the Institut Curie and the French ministry. The animals have been acclimated for at least 7 days prior to commencing experiments, and housed in pathogen-free environment on sawdust in cages of standard dimensions with no more than 6 animals, under controlled conditions of light and dark cycles (12h :12h), relative humidity (55%), and temperature (21°C). Food and tap water were available *ad libitum*. All radiation treatments of animals receiving the combined treatment were performed 5h after AsiDNA administration.

Xenografts. Grafting procedures were performed in adult female NMRI-Foxn1^{nu/nu} mice (Janvier, Le Genest Saint Isle, France) as described in Appendix Supplementary Methods. Treatments cohorts were distributed with homogenous average and variation in tumor size, or total photon count (TC).

Biodistribution studies. Treatments were done at the concentration of 0.24mg/g (1/10 Cy5.5-AsiDNA) via IP (0.9 % NaCl) in 11 days-old pups RjOrl:SWISS and adult NMRI-Foxn1^{nu/nu} mice (Janvier, Le Genest Saint Isle, France). Grafted adults received treatments 18 and 27 days after HDMB03- and U87-*luc* grafts, respectively, or upon appearance of symptoms associated to brain tumor growth. Brains were harvested 4 hours after treatments and Cy5.5 fluorescence imaging on brains with visible tumors was done using Typhoon scanner (GE Healthcare) and image analysis was done with ImageJ software. Cy5.5-AsiDNA plasma concentration of adult NMRI-Foxn1^{nu/nu} was assayed by Victor X3 (PerkinElmer) fluorescence reading.

Toxicity studies. 10 days-old pups RjOrl:SWISS mice (Janvier, Le Genest Saint Isle, France) received 0.75mg/g of AsiDNA via IP (0.9% NaCl). A single dose of 10, 15 or 20 Gy focal cranial irradiation was performed using small animal radiation research platform (SARRP) (XStrahl, Inc.) Plasma circulating growth hormone was assayed by ELISA (Merck Millipore, EZRMGH-45K) 17 days after treatments (27 days of age). MRI experiments were performed at 400 MHz (9.4 T) on a Varian/Agilent scanner approximately 6 months after treatments. Volumes of the lateral and third ventricles were measured using Imaris software (v9.3.1; Bit Plane, Inc.). Femur bone length was measured using a caliper tool (Fisher Scientific) from animals that reached adulthood at their endpoint. Rotarod tests were performed approximately two months after treatments. Further details can be found in Appendix Supplementary Methods.

Efficacy studies. NMRI-Foxn1^{nu/nu} animals bearing subcutaneous and orthotopic grafts started treatments 18 and 12 days after grafts, respectively. AsiDNA treatments were administered every other day in open week days for three weeks (total 9 times). AsiDNA was administered locally with 2 mg: 1 mg subcutaneous + 1 mg intra-tumoral (in 5% glucose) in animals bearing subcutaneous grafts and administered IP with 15mg (in 0.9% NaCl) in animals bearing orthotopic grafts. Subcutaneous xenografts were irradiated with a fractionated dose of 1.8 Gy, using Xrad-320 (Precision X-ray (PXi), Inc) every open day for two (10 fractions) or three weeks (15 fractions). Animals with brain orthotopic grafts received a single dose of focal cranial irradiation of either 6.5 or 10.2 Gy, using SARRP. No apparent morbidities associated to treatment were observed in any treatment cohort or model.

Statistical analysis

Statistical analyzes were carried out using GraphPad Prism (v 7.03). Statistical details can be found in both figures and figure legends. Statistical significance was considered when $p < 0.05$.

Results

AsiDNA can be efficiently distributed to developing brain and brain tumors upon systemic administration

The blood-brain barrier (BBB) is a natural barrier to most systemic chemotherapy drugs and thus an obstacle in the successful development of new treatments for brain tumors. To determine whether AsiDNA reaches the brain, we quantified the brain fluorescence upon intraperitoneal (IP) injection of fluorescent Cy5.5-AsiDNA. Quantifications were performed on brains harvested four hours after treatment, a time corresponding to near complete plasma clearance of AsiDNA (96% clearance from its peak concentration at ~ 0.5 hours) (Supplementary Fig.S1).

Animals without brain tumors (mock-grafted with vehicle solution) showed no accumulation of Cy5.5-AsiDNA in brain tissues. However, Cy5.5-AsiDNA was significantly increased in mice bearing brain tumors of MB (HDMB03, $p=0.0085$) and glioblastoma (U87, $p=0.0027$) (Figure 1A). Interestingly, Cy5.5-AsiDNA intensity was significantly higher at the tumor site compared to normal brain tissues (Figure 1B) ($p=0.0186$, Figure 1C), showing a greater tendency to accumulate in the tumor tissue. Moreover, cellular AsiDNA activity measured by pan-nuclear γ H2AX, was four-times higher in brain tumors than in the surrounding normal tissue (Figure 1D). Our results show that AsiDNA brain bioavailability in the presence of a tumor is due to the BBB alterations elicited by the tumors themselves rather than the grafting mechanical disruption.

Because MB is commonly a pediatric malignancy and the BBB composition differs at the different stages of development (37), we also evaluated the brain permeability of healthy 11-days-old pups to Cy5.5-AsiDNA. Cy5.5-AsiDNA distributed rapidly throughout the body (Figure 1E) and reached the young brain efficiently ($p=0.0261$, Figure 1A) and homogeneously (Figure 1B). Treated brains presented 3.2-times more cells with pan-nuclear γ H2AX than non-treated (NT) (Figure 1F). γ H2AX was not restricted to CD34 blood vessels, indicating that AsiDNA penetrates beyond the BBB of young murine models.

Altogether, our results suggest that AsiDNA can cross the BBB in healthy young brains and reach and disrupt the DNA damage signaling in brain tumor tissues.

No evidence of additional toxicity by AsiDNA in developing models

To estimate the effects of AsiDNA with radiotherapy in young patients, we investigated the impact of combination protocols in 10-days-old pups. To spare radiosensitive organs, such as salivary glands or eyes, from the treatment plan, we used an image-guided small animal irradiator SARRP (Figure 2A). Because of the length of the protocols and the need for continued anesthesia, we assessed the toxicity of a single high-dose brain radiation.

Brain radiation in pups was well tolerated up to doses of 15 Gy, showing no morbidities or evidence of ill-being (Supplementary Fig.S2A and B). Brain radiation with doses of 20 Gy was lethal, with a marked death rate of 71.4% within the first two months and 85.7% eight months after treatment ($p < 0.0001$, Figure 2B). The combination of AsiDNA to 10 and 15 Gy did not affect radio tolerance, as no change in weight or survival was observed (Supplementary Fig.S2A and B). However, when combined to lethal doses of 20 Gy, AsiDNA significantly delayed and spared radiation-associated deaths, presenting a death rate of only 55.6% within the first 80 days after the treatments ($p = 0.0365$), corresponding to 30.1% of animals saved from the lethality of 20 Gy irradiation by AsiDNA administration (Figure 2B).

Growth problems and impaired growth hormone (GH) production are common side effects in childhood cancer survivors who have received large volumes of radiation (10). Animals receiving 20 Gy presented approximately 20% lower average weights (Figure 2C) and significantly shorter femur length ($p = 0.02$, Figure 2D) compared to non-irradiated animals. Consistently, levels of circulating GH 17 days after treatments were ~2.7-fold lower in irradiated animals compared to non-irradiated ($p = 0.0175$, Figure 2E). Treatment with AsiDNA alone did not change weight, femur length ($p = 0.8717$, Figure 2D) and circulating GH ($p = 0.7999$, Figure 2E). Combination of AsiDNA with 20 Gy did not exacerbate the radiation-induced alterations in the assessed parameters (Figure 2C) ($p = 0.1459$, Figure 2D) ($p = 0.7999$, Figure 2E). Our results show no evidence that AsiDNA affects normal development.

To investigate the long-term impact of treatment in brain structures, we performed magnetic resonance imaging (MRI) on the brains of treatment survivors. We observed that animals in all treatment groups presented a moderately larger but non-significant ventricle volume as compared to sham-treated (Figure 2F). Histological analysis showed that irradiated brains present lower myelin levels at the corpus callosum structure (Figure 2G). Myelin rarefaction was only significant in animals receiving radiation alone ($p = 0.0222$, Supplementary Table S2). Overall,

motor performance tests showed that animals receiving sub-lethal doses of radiation remained on the rotarod for less time than other cohorts. Performance of animals receiving only AsiDNA was unaffected (58.2 sec) and in combination with radiation, animals performed similarly to sham-treated times (53.5 sec and 57.6 sec, respectively) (Figure 2H).

Altogether, our results indicate that the combination of AsiDNA with radiation does not exacerbate the toxic effect of brain radiation in both subacute (measured by growth and development) and chronic phases (measured by structural and molecular brain organization and cognition). Moreover, to a modest but significant extent, AsiDNA seemed to protect from radiation-induced death.

Combination of radiotherapy with AsiDNA is more effective than dose escalation

We evaluated whether AsiDNA could improve radiation therapeutic outcomes in high-risk MB, a subset with dismal prognosis (2). We used two models of HDMB03, a cell line that recapitulates key features of Group 3 MB (31) – the most refractory group – and two doses of radiation.

We first tested treatment protocols in animals bearing orthotopic grafts of *luciferase*-expressing HDMB03 (HDMB03-*luc*), for higher anatomic accuracy. AsiDNA was administered by IP injection, and the grafting area of the brain was irradiated with a single dose of 6.5 Gy or 10.2 Gy (Figure 3A). To avoid radiation-mediated morbidities that could affect animal survival and compromise the assessment of the efficacy of treatments, we used image-guided SARRP brain radiation to exclude radiosensitive tissues from the radiation plan. We observed that 6.5 and 10.2 Gy significantly increased survival by 10 and 12 days, respectively ($p < 0.0001$, Figure 3B). Interestingly, the increase in radiation dose from 6.5 to 10.2 Gy did not significantly improve survival rates ($p = 0.0602$). AsiDNA alone increased survival moderately but significantly, by 2 days compared to NT ($p = 0.0496$). The combination of AsiDNA to low-dose radiation of 6.5 Gy increased median survival by 2.5 days compared to the 6.5 Gy-only counterpart (Supplementary Fig.S3A). AsiDNA treatments improved the magnitude and prolonged the length duration of the response of tumors to treatment (Figure 3C, Supplementary Fig.S3B). These results confirm the ability of AsiDNA to reach brain tumor tissues at effective therapeutic doses via systemic administration. With the exception of one animal, histological analysis showed no obvious enhancement of apoptosis by AsiDNA (Supplementary Fig.S3C).

Because these fractionated radiation protocols are not technically compatible with SARRP focal brain irradiation, we used animals bearing subcutaneous HDMB03 grafts, to recapitulate fractionated radiotherapy protocols with dose/fractions of 1.8 Gy. Animals received local injections of AsiDNA and two different radiation doses: 1.8 Gy in 10 fractions, total dose of 18 Gy, and in 15 fractions, total dose of 27 Gy (Figure 3D). Both radiation protocols significantly delayed tumor growth ($p < 0.0001$, Supplementary Fig.S3D) and improved survival, respectively ($p < 0.0001$, Figure 3E). Interestingly, the increase by 50% of the total radiation dose from 18 Gy to 27 Gy did not significantly improve tumor growth control ($p = 0.0889$, Supplementary Fig.S3D) nor survival ($p = 0.6719$, Figure 3E). When treated with 27 Gy, the total number of responders only increased by 10% (Supplementary Fig.S3E). These results suggest that maximal efficacy of fractionated radiation is reached after 10 fractions. AsiDNA alone had a mild but significant effect on subcutaneous tumor growth control ($p = 0.0193$, Supplementary Fig.S3D) and on survival, extending it 7.5 days compared to mock-treated ($p = 0.0085$, Figure 3F). When combined with fractionated radiation, AsiDNA increased median survival by 17 days as compared to radiation-only, no matter the total irradiation dose, overcoming the irradiation maximal efficacy (Supplementary Fig.S3F). Median tumor change (Supplementary Fig.S3E) and the length duration of the response of tumors to treatment (Figure 3F) were improved by AsiDNA. Furthermore, the gain in median survival with the addition of AsiDNA to the 18 Gy treatment was superior to the gain provided by the 50% increase of radiation dose to 27 Gy.

Altogether, orthotopic and subcutaneous models of HDMB03 models displayed similar responses to AsiDNA and radiation treatments, independent of the delivery protocols, providing evidence for the robustness of our observations. Our results demonstrate that the addition of AsiDNA to radiation improves treatment outcomes more effectively than increasing radiation doses.

AsiDNA treatments enhance MB cells' radiosensitivity irrespective of their genetic background

As the different MB groups and certain genetic alteration profiles diverge in their treatment response in clinics (2), we investigated the differential sensitivity to AsiDNA treatment of different MB cell lines. We used a panel of four MB cell lines from different molecular groups

(SHH and Group 3) and *TP53* status (wt, wild type; mut, mutated), and analyzed their proliferation and death upon treatment.

As expected, *TP53* status predicted MB cell lines' radiosensitivity; *TP53* wt cell lines HDMB03 and ONS76 were more radiosensitive (half-maximal dose survival (D_{50}) = 1.7 and 3.4 Gy, respectively), than *TP53* mut DAOY (D_{50} = 4.2 Gy) and UW228.1 (D_{50} = 4.8 Gy) (Figure 4A and D). These observations meet the prognostic value of *TP53* in MB, especially in SHH-MB, as SHH-MB harboring aberrations in the *TP53* gene have poorer treatment response and dismal prognosis (38). In contrast to intrinsic radiosensitivity, the effect of AsiDNA-alone treatment was independent of the *TP53* status or molecular group, as all four cell lines were sensitive to AsiDNA in a significant and dose-dependent manner (Figure 4A). The reduction in survival obtained from the addition of AsiDNA to 2 Gy, similar to the median doses practiced in clinical fractionated protocols (5), is significantly greater than the impact of increasing radiation alone (Supplementary Table S1). AsiDNA treatments decreased the survival fraction in a cytotoxic manner, increasing the percentage of cell death relative to the radiation counterpart in all cell lines (Figure 4A).

Because of the common emergence of *TP53* mutations at relapse and the almost universal failure to treat MB recurrence (39), we tested the radiosensitizing effect of AsiDNA in HDMB03-sh*TP53* depleted for *TP53* expression. HDMB03-sh*TP53* c05 cells expressed 1.43-times lower levels of p53 protein upon radiation and failed to activate their downstream target p21 (Figure 4B). *TP53* depletion induced a 1.6-fold change in radioresistance, increasing the dose required to kill 50% of cells population (D_{50}) from 2.1 Gy in HDMB03-shControl to 3.3 Gy in HDMB03-sh*TP53* (Figure 4C and D). Treatment combinations of AsiDNA with radiation bypassed the radioresistance mediated by *TP53* depletion, showing similar D_{50} to those of HDMB03-shControl for both doses of AsiDNA (Figure 4C and D). These results confirm that AsiDNA does not rely on *TP53* to increase radiation sensitivity.

In conclusion, the cytotoxicity of AsiDNA treatments appears to be independent of the MB intrinsic radiosensitivity, molecular group and *TP53* status.

AsiDNA induces similar changes and potentiates the expression programs involved in the response to radiation

To understand how AsiDNA treatments confer comparable radiosensitization across cell lines that respond differently to radiation, we performed RNA-Seq analysis in HDMB03 (*TP53* wt, Group 3, $D_{50}=1.7$ Gy) and in DAOY (*TP53* mut, SHH group, $D_{50}= 4.2$ Gy). Both cell lines were treated with AsiDNA and radiation doses of 1.8 Gy and 6 Gy.

Principal component analysis (PCA) demonstrated that HDMB03 and DAOY cluster separately, and 94.8% of the variability in the sample is associated with the cell of origin (Supplementary Fig.S4A). Fold-change expression upon 6 Gy radiation or AsiDNA against NT samples showed no correlation in treatment response between the two cell lines ($r=0.12$ and $r=0.05$, respectively) (Figure 5A). Basal and treatment-response expression patterns in HDMB03 and DAOY differed drastically. However, the expression profiles of AsiDNA and 6 Gy radiation correlated significantly in each cell line ($r=0.72$ and $r=0.64$ for HDMB03 and DAOY, respectively) (Figure 4B). These results suggest that AsiDNA-mediated transcriptional response mirrors the cell-specific response modulated by irradiation.

Hierarchical clustering was used to identify subsets of genes showing coordinated expression changes at increasing doses of radiation: eight clusters were identified for HDMB03, and seven for DAOY. Among these clusters, clusters 3 and 5 in HDMB03 and clusters 2 and 4 in DAOY showed the strongest expression of dose-dependent regulation (Supplementary Fig.S4B and C). In HDMB03, cluster 3 consists of down-regulated genes involved in cell cycle progression, whereas cluster 5 comprises up-regulated genes involved in p53-mediated pathways and others regulating cell fate, death, progression, differentiation and cellular inflammation that are up-regulated (Figure 5C). In DAOY, cluster 2 consists of down-regulated genes regulating epithelial-mesenchymal transition, whereas cluster 4 comprises up-regulated genes involved in cellular inflammation (Figure 5E). Differences between regulated pathways in response to radiation in both cell lines are likely due to their *TP53* status. In these defined clusters, AsiDNA alone lead to a regulation of the same set of genes as a 1.8 Gy dose. Combining AsiDNA and radiation further enhances expression of these genes and is comparable to increasing radiation doses in both HDMB03 and DAOY.

Expression values of key effector genes in these pathways help one understand the impact of the combined treatments. *CDKN1A* (p21), with roles on cell cycle arrest; *BBC3* (PUMA), an inducer of apoptosis; and *GADD45A*, regulator of DNA repair, can serve as an example of the additive

endorsement of AsiDNA to the transcriptional radio response in HDMB03 (Figure 5D). Moreover, the number of significantly up-regulated genes in the p53 pathway does not change with increasing radiation doses, whereas adding AsiDNA to 1.8 and 6 Gy increases this number from 20 to 22 and 26, respectively. In DAOY, *CXCL1* (C-X-C Motif Chemokine Ligand 1), *IL1A* (Interleukin 1 α) and *IFIT2* (Interferon Induced Protein With Tetratricopeptide Repeats 2) show AsiDNA-mediated additivity (Figure 5F). Both radiation doses promote a regulation change in seven of the TNF α pathway genes set, whereas a combination of AsiDNA increased the number of overlapping genes from 7 to 13 and 28 in 1.8 and 6 Gy doses, respectively (Supplementary Fig.S4D).

Our results indicate that AsiDNA modulates the expression of the same cell-specific pathways that are activated in response to radiation and reinforces their transcriptional response, as do higher radiation doses. The pathways showing the strongest regulation on radiation in HDMB03 and DAOY are associated with cell death programs, such as p53 and TNF α , respectively.

AsiDNA-mediated DNA repair inhibition increases markers of genetic instability, reinforcing radiation-mediated cytotoxicity, favoring necrotic cell death

To understand the cytotoxic impact of the AsiDNA-mediated radio-mimicking transcriptional response in MB, we evaluated the type of cell death induced in HDMB03 and DAOY upon irradiation, and AsiDNA. Upon irradiation, both HDMB03 and DAOY activate apoptotic death (Figure 6A), whereas necrosis is increased only in HDMB03. The necrotic fraction is further increased when AsiDNA is associated with radiation in both cell lines. Interestingly, the preferential irradiation-induced cell death in DAOY cells is apoptosis with or without AsiDNA (Figure 6A). Thus, AsiDNA seems to increase necrosis, independent of the genetic background and the radiation-induced cell death pathway.

In previous works, the mechanisms of DNA repair inhibition by AsiDNA have been thoroughly characterized in adult tumor models, which are often deficient in *TP53* and have high degree of genetic instability. To evaluate the impact of AsiDNA on the major DSB repair pathways in a pediatric cancer model, we assessed the ability of HDMB03 (*TP53* wt) to form foci of non-overlapping repair factors after radiation, such as 53BP1, involved in non-homologous end-joining repair, and BRCA1, involved in homologous recombination repair. As expected, radiation alone led to a significant increase of foci formation of 53BP1 and BRCA1, ($p < 0.0001$)

(Figure 6B and C). In both cell lines, AsiDNA induced, as previously reported, a characteristic pan-nuclear γ H2AX that persisted in irradiated cells (Figure 6B and C). Recruitment of 53BP1 and BRCA1 was significantly inhibited after irradiation in cells treated with AsiDNA, as shown by the decrease of 1.4 and 2-fold, respectively, in the mean number of foci formed by 53BP1 ($p=0.0097$) and BRCA1 ($p<0.0001$) after irradiation (Figure 6B and C). The inhibition of DNA repair factor recruitment by AsiDNA upon irradiation is independent of the *TP53* status, and the mechanism of AsiDNA DNA repair inhibition are conserved in pediatric tumors.

Micronuclei are a universal marker of genomic instability (40) and a predictive biomarker of AsiDNA sensitivity (36). To evaluate the consequences of the AsiDNA-mediated DNA repair inhibition in MB, we assessed the frequency of micronuclei 72 hours after low radiation treatments of 1.8 Gy in HDMB03 (*TP53* wt) and DAOY (*TP53* mut). Radiation significantly increased the frequency of micronuclei 3.2- and 1.6-fold in HDMB03 and in DAOY, respectively ($p=0.0002$ and $p<0.0001$, respectively) (Figure 6D). Compared to NT, AsiDNA led to a 1.8- and 1.6-fold increase in micronucleated cells in both HDMB03 and DAOY ($p=0.0575$ and $p<0.0001$, respectively), making the effect in DAOY as strong as the effect of radiation. When combined with radiation, AsiDNA led to a further increase of the frequency of micronuclei in an additive manner (Figure 6D). These observations corroborate the observations that AsiDNA impairs repair of radiation genotoxic insults. The increase of micronucleated cells suggests that AsiDNA could kill cells through mitotic accident, leading to necrotic death, favoring a more protracted and continuous cytotoxic effect over the one provided by radiation alone.

Discussion

Contrary to other pediatric cancers, various reports show that MB survivors still show a high-risk of morbidity (13). For more than 25 years, no new drugs have been approved by the food and drug administration for treatment of pediatric brain tumors (41). To our knowledge, our studies is one of the few MB preclinical studies that have tested the combination of new approaches to conventional therapies, in addition to comprehensively analyzing and describing both the efficacy and toxicity of the proposed protocols. Two protocols using either fractionated irradiation on subcutaneous tumors or single-dose brain irradiation were employed because, due to technical challenges, focal brain irradiation could not be safely repeated on small animals. Nonetheless, the applicability of the protocols and models used was validated by the reproduction of the various clinically described adverse effects caused by childhood brain irradiation and by the similar observations of treatment efficacy in both models and protocols.

The various assessments at subacute and chronic periods after treatment did not show that AsiDNA added toxicity to the effects caused by brain irradiation. In contrast, animals receiving a combination of treatments showed better survival than their radiation-only counterparts. The absence of added toxicity with AsiDNA has already been reported in various studies using adult models in association with radiotherapy (22, 25, 27), doxorubicin (18, 21), carboplatin (26) and oxaliplatin and 5-fluorouracil (24). The clinical trial DRIIM (NCT01469455) demonstrated that combining AsiDNA with radiotherapy does not increase radiation-induced skin toxicity in patients (29). The mechanism underlying the AsiDNA specificity for tumor tissues is not yet fully understood. The low distribution of the drug and poor activation of AsiDNA targets (pan-nuclear γ H2AX) within the healthy tissues surrounding the tumor suggest that distribution and activity of AsiDNA occurs preferentially within tumor tissues.

The use of two different models in the high-risk Group 3 MB provided robust information on the radiosensitizing properties of AsiDNA, indicating that AsiDNA efficacy is independent of the radiation doses and protocols – fractionated or single-dose – or route of administration – local or systemic. AsiDNA increased the time tumors responded to treatment, resulting in improvement of median survival, validating the ability of AsiDNA to penetrate the brain tumor tissues at efficient doses by systemic administration. Interestingly, the combination of AsiDNA with low radiation doses showed better outcomes than increasing radiation doses. As such, AsiDNA could

help achieve the same therapeutic benefits with lower radiation doses, mitigating dose-dependent adverse effects of radiation.

Treatment additivity is preferable in the pediatric oncology realm, as frequently they do not show overlapping toxicities (42, 43). In vitro studies demonstrated that the mostly additive radiosensitizing effect of AsiDNA is not restricted to Group 3 MB but applies across different molecular groups, irrespective of intrinsic radiosensitivity, genetic background or *TP53* status. Mutations on *TP53* commonly emerge at MB relapse, conferring radioresistance to the recurring tumor (44). Using a *TP53*-silenced model, we demonstrated that AsiDNA can in fact reverse the radioresistance induced by *TP53* loss. It would be interesting to further explore the potential of AsiDNA to increase treatment response in recurrent MB, for which there is no available treatment (39).

Some have proposed that targeted therapies with a broader spectrum of action could offer new hope in pediatric oncology care (45) because low rates of mutations and contrasting differences across groups limit options for rational and targeted therapy (46-48). Mechanistic insights into the AsiDNA broad spectrum of radiosensitization suggest that the cytotoxic outcome of AsiDNA is the result of a two-way operation: (i) on one hand, AsiDNA increases the number of key factors involved in programmed cell death and their expression, as do higher radiation doses without evoking real DNA damage; (ii) on the other hand, the DNA repair inhibitor AsiDNA hampers the cell's attempt to repair the DNA damage induced by radiation. The mostly additive cytotoxic nature of AsiDNA is not reliant on a programmed cascade of events or on a single pathway and is able to directly and indirectly reinforce the tumor radiation (Figure 6E).

Here, we present preclinical evidence that the brain-penetrant DNA repair inhibitor AsiDNA is a potential candidate to improve radiotherapy efficacy in MB models without added toxicity. AsiDNA has great potential for clinical translation in pediatric clinical testing as clinical trials have demonstrated AsiDNA to be well tolerated and safe in combination with radiotherapy. Radiosensitization by AsiDNA may help address a significant unmet clinical need in MB care by augmenting treatment efficacies and consequently improving clinical outcomes in high-risk subsets and by allowing for radiation de-escalation in standard-risk patients, thus mitigating dose-dependent morbidities. Protocols used throughout this study could be translated for other

pediatric cancers for higher therapeutic benefits, especially considering the genetic background-independent activity of this drug.

Acknowledgements

This work was supported by the PIC3i-Curie, the Institut Curie and the IRS “NanoTheRad” of University Paris-Sud (Paris-Saclay). SF was supported by a Marie Skłodowska-Curie European fellowship ITN-RADIATE No. 642623 and, by the *Espoirs de la recherche* program from *Fondation pour la Recherche Médicale* (FRM) No. FDT201805005345. AG was supported by the Horizon 2020 Framework Programme for Research and Innovation (H2020 Marie Skłodowska-Curie Actions grant agreement No. 798106 “REPLICHRM4D”). The authors greatly acknowledge Victoria Djordjevic for her help in the in vivo work; Dr. Genevieve Almouzni Institut Curie- UMR 3664 for her contribution in the development of the RNA-Seq data analysis with Alberto Gatto; Nathalie Berthault for her help in analyzing the in vivo data; Christophe Alberti and Elodie Belloir for their work at the mouse facilities; Sophie Leboucher for her work on the histology; Charlene Lasgi for her help on FACS analysis; David Wasilewski for the discussions and advices on the toxicity studies; the RadExp platform for performing all the animal irradiation and Cédric Messaoudi from Institut Curie UMR9187/U1196 and Laetitia Besse from the PICT-IBiSA Imaging Facility for useful advices on image processing.

References

1. Ostrom QT, Gittleman H, Truitt G, Boscia A, Kruchko C, Barnholtz-Sloan JS. CBTRUS Statistical Report: Primary Brain and Other Central Nervous System Tumors Diagnosed in the United States in 2011-2015. *Neuro Oncol.* 2018;20(suppl_4):iv1-iv86.
2. Northcott PA, Korshunov A, Pfister SM, Taylor MD. The clinical implications of medulloblastoma subgroups. *Nat Rev Neurol.* 2012;8(6):340-51.
3. Ramaswamy V, Remke M, Bouffet E, Bailey S, Clifford SC, Doz F, et al. Risk stratification of childhood medulloblastoma in the molecular era: the current consensus. *Acta Neuropathol.* 2016;131(6):821-31.
4. Packer RJ, Vezina G. Management of and prognosis with medulloblastoma: therapy at a crossroads. *Arch Neurol.* 2008;65(11):1419-24.
5. Northcott PA, Robinson GW, Kratz CP, Mabbott DJ, Pomeroy SL, Clifford SC, et al. Medulloblastoma. *Nat Rev Dis Primers.* 2019;5(1):11.
6. Paterson E, Farr RF. Cerebellar medulloblastoma: treatment by irradiation of the whole central nervous system. *Acta radiol.* 1953;39(4):323-36.
7. Moxon-Emre I, Bouffet E, Taylor MD, Laperriere N, Scantlebury N, Law N, et al. Impact of craniospinal dose, boost volume, and neurologic complications on intellectual outcome in patients with medulloblastoma. *J Clin Oncol.* 2014;32(17):1760-8.
8. Vatner RE, Niemierko A, Misra M, Weyman EA, Goebel CP, Ebb DH, et al. Endocrine Deficiency As a Function of Radiation Dose to the Hypothalamus and Pituitary in Pediatric and Young Adult Patients With Brain Tumors. *J Clin Oncol.* 2018;36(28):2854-62.
9. Palmer SL, Armstrong C, Onar-Thomas A, Wu S, Wallace D, Bonner MJ, et al. Processing speed, attention, and working memory after treatment for medulloblastoma: an international, prospective, and longitudinal study. *J Clin Oncol.* 2013;31(28):3494-500.
10. Bereket A. Endocrinologic Consequences of Pediatric Posterior Fossa Tumours. *J Clin Res Pediatr Endocrinol.* 2015;7(4):253-9.
11. Schreiber JE, Palmer SL, Conklin HM, Mabbott DJ, Swain MA, Bonner MJ, et al. Posterior fossa syndrome and long-term neuropsychological outcomes among children treated for medulloblastoma on a multi-institutional, prospective study. *Neuro Oncol.* 2017;19(12):1673-82.
12. Moxon-Emre I, Bouffet E, Taylor MD, Laperriere N, Sharpe MB, Laughlin S, et al. Vulnerability of white matter to insult during childhood: evidence from patients treated for medulloblastoma. *J Neurosurg Pediatr.* 2016;18(1):29-40.
13. Salloum R, Chen Y, Yasui Y, Packer R, Leisenring W, Wells E, et al. Late Morbidity and Mortality Among Medulloblastoma Survivors Diagnosed Across Three Decades: A Report From the Childhood Cancer Survivor Study. *J Clin Oncol.* 2019;37(9):731-40.
14. Dutreix M, Devun F, Herath N, Noguez-Hellin P. Dbait: A New Concept of DNA Repair Pathways Inhibitor from Bench to Bedside. In: Pollard J, Curtin N, editors. *Targeting the DNA Damage Response for Anti-Cancer Therapy.* Cham: Springer International Publishing; 2018. p. 359-73.
15. Croset A, Cordelieres FP, Berthault N, Buhler C, Sun JS, Quanz M, et al. Inhibition of DNA damage repair by artificial activation of PARP with siDNA. *Nucleic Acids Res.* 2013;41(15):7344-55.
16. Quanz M, Chassoux D, Berthault N, Agrario C, Sun JS, Dutreix M. Hyperactivation of DNA-PK by double-strand break mimicking molecules disorganizes DNA damage response. *PLoS One.* 2009;4(7):e6298.
17. Quanz M, Berthault N, Roulin C, Roy M, Herbette A, Agrario C, et al. Small-molecule drugs mimicking DNA damage: a new strategy for sensitizing tumors to radiotherapy. *Clin Cancer Res.* 2009;15(4):1308-16.

18. Herath NI, Devun F, Herbette A, Lienafa MC, Chouteau P, Sun JS, et al. Potentiation of doxorubicin efficacy in hepatocellular carcinoma by the DNA repair inhibitor DT01 in preclinical models. *Eur Radiol.* 2017.
19. Jdey W, Thierry S, Russo C, Devun F, Al Abo M, Noguez-Hellin P, et al. Drug-Driven Synthetic Lethality: Bypassing Tumor Cell Genetics with a Combination of AsidDNA and PARP Inhibitors. *Clin Cancer Res.* 2017;23(4):1001-11.
20. Herath NI, Devun F, Lienafa MC, Herbette A, Denys A, Sun JS, et al. The DNA Repair Inhibitor DT01 as a Novel Therapeutic Strategy for Chemosensitization of Colorectal Liver Metastasis. *Mol Cancer Ther.* 2016;15(1):15-22.
21. Devun F, Herath N, Denys A, Sun J-s, Dutreix M. DNA repair inhibition by DT01 as an adjuvant therapy at each stage of hepatocellular cancer (HCC) treatment. *Journal of Clinical Oncology.* 2015;33(3_suppl):303-.
22. Biau J, Devun F, Jdey W, Kotula E, Quanz M, Chautard E, et al. A preclinical study combining the DNA repair inhibitor Dbait with radiotherapy for the treatment of melanoma. *Neoplasia.* 2014;16(10):835-44.
23. Devun F, Biau J, Huerre M, Croset A, Sun JS, Denys A, et al. Colorectal cancer metastasis: the DNA repair inhibitor Dbait increases sensitivity to hyperthermia and improves efficacy of radiofrequency ablation. *Radiology.* 2014;270(3):736-46.
24. Devun F, Bousquet G, Biau J, Herbette A, Roulin C, Berger F, et al. Preclinical study of the DNA repair inhibitor Dbait in combination with chemotherapy in colorectal cancer. *J Gastroenterol.* 2012;47(3):266-75.
25. Thierry S, Jdey W, Alculumbre S, Soumelis V, Noguez-Hellin P, Dutreix M. The DNA Repair Inhibitor Dbait Is Specific for Malignant Hematologic Cells in Blood. *Mol Cancer Ther.* 2017;16(12):2817-27.
26. Herath NI, Berthault N, Thierry S, Jdey W, Lienafa MC, Bono F, et al. Preclinical Studies Comparing Efficacy and Toxicity of DNA Repair Inhibitors, Olaparib, and AsidDNA, in the Treatment of Carboplatin-Resistant Tumors. *Front Oncol.* 2019;9:1097.
27. Coquery N, Pannetier N, Farion R, Herbette A, Azurmendi L, Clarencon D, et al. Distribution and radiosensitizing effect of cholesterol-coupled Dbait molecule in rat model of glioblastoma. *PLoS One.* 2012;7(7):e40567.
28. Biau J, Chautard E, Berthault N, de Koning L, Court F, Pereira B, et al. Combining the DNA Repair Inhibitor Dbait With Radiotherapy for the Treatment of High Grade Glioma: Efficacy and Protein Biomarkers of Resistance in Preclinical Models. *Front Oncol.* 2019;9:549.
29. Le Tourneau C, Dreno B, Kirova Y, Grob JJ, Jouary T, Dutriaux C, et al. First-in-human phase I study of the DNA-repair inhibitor DT01 in combination with radiotherapy in patients with skin metastases from melanoma. *Br J Cancer.* 2016;114(11):1199-205.
30. Waszak SM, Northcott PA, Buchhalter I, Robinson GW, Sutter C, Groebner S, et al. Spectrum and prevalence of genetic predisposition in medulloblastoma: a retrospective genetic study and prospective validation in a clinical trial cohort. *Lancet Oncol.* 2018;19(6):785-98.
31. Milde T, Lodrini M, Savelyeva L, Korshunov A, Kool M, Brueckner LM, et al. HD-MB03 is a novel Group 3 medulloblastoma model demonstrating sensitivity to histone deacetylase inhibitor treatment. *J Neurooncol.* 2012;110(3):335-48.
32. Keles GE, Berger MS, Srinivasan J, Kolstoe DD, Bobola MS, Silber JR. Establishment and characterization of four human medulloblastoma-derived cell lines. *Oncol Res.* 1995;7(10-11):493-503.
33. Garancher A, Lin CY, Morabito M, Richer W, Rocques N, Larcher M, et al. NRL and CRX Define Photoreceptor Identity and Reveal Subgroup-Specific Dependencies in Medulloblastoma. *Cancer Cell.* 2018;33(3):435-49 e6.

34. Biau J, Chautard E, Court F, Pereira B, Verrelle P, Devun F, et al. Global Conservation of Protein Status between Cell Lines and Xenografts. *Transl Oncol.* 2016;9(4):313-21.
35. Rocques N, Abou Zeid N, Sii-Felice K, Lecoin L, Felder-Schmittbuhl MP, Eychene A, et al. GSK-3-mediated phosphorylation enhances Maf-transforming activity. *Mol Cell.* 2007;28(4):584-97.
36. Jdey W, Thierry S, Popova T, Stern MH, Dutreix M. Micronuclei Frequency in Tumors Is a Predictive Biomarker for Genetic Instability and Sensitivity to the DNA Repair Inhibitor AsiDNA. *Cancer Res.* 2017;77(16):4207-16.
37. Engelhardt B, Liebner S. Novel insights into the development and maintenance of the blood-brain barrier. *Cell Tissue Res.* 2014;355(3):687-99.
38. Zhukova N, Ramaswamy V, Remke M, Pfaff E, Shih DJ, Martin DC, et al. Subgroup-specific prognostic implications of TP53 mutation in medulloblastoma. *J Clin Oncol.* 2013;31(23):2927-35.
39. Johnston DL, Keene D, Strother D, Taneva M, Lafay-Cousin L, Fryer C, et al. Survival Following Tumor Recurrence in Children With Medulloblastoma. *J Pediatr Hematol Oncol.* 2018;40(3):e159-e63.
40. Fenech M, Kirsch-Volders M, Natarajan AT, Surralles J, Crott JW, Parry J, et al. Molecular mechanisms of micronucleus, nucleoplasmic bridge and nuclear bud formation in mammalian and human cells. *Mutagenesis.* 2011;26(1):125-32.
41. Aldape K, Brindle KM, Chesler L, Chopra R, Gajjar A, Gilbert MR, et al. Challenges to curing primary brain tumours. *Nat Rev Clin Oncol.* 2019;16(8):509-20.
42. Berg SL, Grisell DL, DeLaney TF, Balis FM. Principles of treatment of pediatric solid tumors. *Pediatr Clin North Am.* 1991;38(2):249-67.
43. Taylor RE. Cancer in children: radiotherapeutic approaches. *Br Med Bull.* 1996;52(4):873-86.
44. Hill RM, Kuijper S, Lindsey JC, Petrie K, Schwalbe EC, Barker K, et al. Combined MYC and P53 defects emerge at medulloblastoma relapse and define rapidly progressive, therapeutically targetable disease. *Cancer Cell.* 2015;27(1):72-84.
45. Adamson PC, Houghton PJ, Perilongo G, Pritchard-Jones K. Drug discovery in paediatric oncology: roadblocks to progress. *Nat Rev Clin Oncol.* 2014;11(12):732-9.
46. Vogelstein B, Papadopoulos N, Velculescu VE, Zhou S, Diaz LA, Jr., Kinzler KW. Cancer genome landscapes. *Science.* 2013;339(6127):1546-58.
47. Roussel MF, Stripay JL. Epigenetic Drivers in Pediatric Medulloblastoma. *Cerebellum.* 2018;17(1):28-36.
48. Huether R, Dong L, Chen X, Wu G, Parker M, Wei L, et al. The landscape of somatic mutations in epigenetic regulators across 1,000 paediatric cancer genomes. *Nat Commun.* 2014;5:3630.

Figure 1 - Brain bioavailability of AsiDNA in developing models and animals bearing orthotopic brain tumors. (A) Cy5.5 average fluorescence intensity relative to NT brain background, scanned on harvested brains 4h after administration of Cy5.5-AsiDNA through IP injection in adult models bearing or not orthotopic grafts (mock-grafts, HDMB03-*luc* or U87-*luc*) and in 11 days-old pups (young brain). Significance tested by Welch T-test (B) Representative brain Cy5.5 fluorescent scan of the conditions mentioned above in (A). Black arrows indicate the grafting site. (C) Comparison of Cy5.5 mean fluorescence present in the brain tissue and the tumor per animal. Significance tested by paired T-test. (D) Representative brain immunofluorescence, stained for γ H2AX (green) and nuclei stained with DAPI (blue) after AsiDNA IP injection in adult brain with tumor (normal tissue, left of white line; tumor tissue, right of white line); numbers indicate number of γ H2AX positive nucleus in both tissues. (E) Live fluorescence imaging of Cy5.5-AsiDNA distribution 1 and 4h after IP injection in pups. Radiant efficiency scale from minimum (2.38×10^{10}) to maximum (6.86×10^{11}). (F) Representative brain immunofluorescence, stained for CD34 (red) and γ H2AX (green) and nuclei stained with DAPI (blue) after AsiDNA IP injection in 11 days-old pups. Numbers represent the mean total number of γ H2AX positive nucleus and of which do not co-localize with CD34 staining \pm standard deviation (n=3). (D, F) Scale bar = 200 μ m. Significance: non-significant, ns; * p<0.05 and ** p<0.01.

Figure 2 – No increase of radiation toxicity with AsiDNA treatment in young models. 10 days-old pups received 0.75mg/g of AsiDNA via intraperitoneal IP and SARRP brain irradiation of 10, 15 or 20 Gy;(A) upper panel, dose-distribution (colored) of the irradiated volume superimposed to the CT-scan image guidance; lower panel, representation of alopecia in the irradiated area 7 days after treatment. (B) Kaplan-Meier representation of animal surviving fraction. Significance given by Logrank test. (C) Mean weight in grams \pm SD, over time after treatments. Period of time without death events highlighted by the green rectangle. (B and C: sham-treated, n=12; 20 Gy, n=14; AsiDNA, n=13; AsiDNA + 20 Gy, n=12). (D) Mean femur length in mm measured from animals that reached adulthood. (E) Mean circulating GH 17 days after treatments, measured by ELISA. (F) Log10 mean volume of the brain ventricles approximately 6 months after treatments (upper panel) and representative brain MRI highlighting in yellow the measured structures, corresponding to the lateral and third brain ventricles (lower panel). (G) Fold-change of Luxol Fast Blue intensity for myelin quantification in corpus callosum brain structures 8 months after treatments (normalized to the sham-treated values) (upper panel) and representative histological sections (lower panel). Scale bar = 300 μ m. (H) Mean rotarod performance two months after treatments represented in minutes (min). (D-H) cohorts receiving AsiDNA treatments are represented in

orange, cohorts without AsiDNA are represented in blue. Significance given by two-way ANOVA test and represented below bar plots. Significance: non-significant, ns; * $p < 0.01$; **** $p < 0.0001$.

Figure 3 – AsiDNA treatments improve radiotherapy efficacy in high-risk medulloblastoma.

Animals bearing orthotopic grafts of HDMB03 (**A, B, C**) or subcutaneous grafts of HDMB03-*luc* (**D, E, F**) received the represented treatment plan (A, D, respectively): (**A**) single brain irradiation with doses of 6.5 Gy or 10.2 Gy, with IP injections of AsiDNA of 9x 2mg, 3x/week for 3 weeks (w); (**D**) fractionated treatment, with 10 or 15 fractions of flank irradiation (yellow circles) of 1.8 Gy and local AsiDNA treatments (red squares) of 2mg, 3x/week for 3 weeks (w); (**B, E**) Kaplan-Meier representation of percentage of living fraction of animals (B: NT, n=17; 6.5 Gy, n= 19, 10.2 Gy, n=10; AsiDNA, n= 10; AsiDNA+6.5Gy, n=10; E: n=10 in each treatment arm). Significance given by Logrank test. Significance: not significant, ns; * $p < 0.05$; ** $p < 0.01$; *** $p < 0.001$ and **** $p < 0.0001$. (**C, F**) Median duration in days of orthotopic (C) and subcutaneous (F) tumor response to treatments in days.

Figure 4 - AsiDNA treatments radiosensitize medulloblastoma cell lines in a cytotoxic manner regardless TP53 status and molecular group.

Survival to AsiDNA (0, light grey circle; 4.8, dark grey square; or 15.9 μ M, black diamond), radiation (0, 2 or 6 Gy), or both was monitored 6 days after treatment by Trypan Blue cell counting in medulloblastoma cell lines (HDMB03, ONS76, DAOY, UW228.1, HDMB03-shControl, HDMB03-sh*TP53*). (**A**) upper panel, percentage of living cells relative to non-treated (NT) condition; lower panel, percentage of cell death relative to total cells. Data are expressed as mean \pm SD of three independent cultures. Detailed significance is presented in Supplementary Table S1. (**B**) Validation of *TP53* knockdown by western blot detection of overall protein levels of p53 and its direct target p21 in HDMB03 parental, HDMB03-shControl (shCtr) and HDMB03-sh*TP53* mass culture c02 and c05 six hours after 6 Gy radiation. (**C**) Efficacy of AsiDNA (0, 4.8 or 15.9 μ M), radiation (0, 2 or 6Gy), or both was monitored 6 days after treatment by Trypan Blue cell counting in HDMB03-shControl and HDMB03-sh*TP53* c05. Data are expressed as mean \pm SD of three independent cultures. (**D**) Calculated dose in Gy leading to 50% survival (D_{50}), with or without AsiDNA (0, 4,8 and 15.9 μ M) given by a linear regression model. Numbers indicate the maximal D_{50} difference observed after AsiDNA treatment.

Figure 5 - AsiDNA induces similar changes and potentiates the cell-specific expression programs involved in radiation response.

(**A**) Comparison of transcriptional changes in response to radiation and AsiDNA in HDMB03 and DAOY. The plot shows the average \log_2 fold change after 6.0Gy (left panel)

and AsiDNA (right panel) for all genes expressed in both HDMB03 (x-axis) and DAOY (y-axis) relative to NT. **(B)** Comparison of transcriptional changes in response to radiation and AsiDNA in HDMB03 (left panel) and DAOY (right panel) for all genes expressed upon 6 Gy radiation (y-axis) and AsiDNA (x-axis) relative to NT. Significantly differentially expressed genes are highlighted in their respective colors (significant at FDR < 1%). The Pearson correlation coefficient for differentially expressed genes is shown on top (r). **(C, E)** Violin plots show the distribution of relative expression levels across all genes in cluster 3 (top down-regulated, left panel) and 5 (top up-regulated, right panel) for HDMB03 (C), and in cluster 2 (top down-regulated, left panel) and 4 (top up-regulated, right panel) for DAOY (E). Each dot represents the average expression of a single gene in a given condition relative to NT conditions. The top 5 enriched hallmark signatures (MSigDB) are shown for both clusters above each panel, along with the corresponding enrichment ratio in parenthesis. Significantly overrepresented signatures at 10% FDR are highlighted in dark bold. The top 5 enriched hallmark signatures (MSigDB) are shown for both clusters above each panel, along with the corresponding enrichment ratio. Significantly overrepresented signatures at 10% FDR are highlighted in dark bold and filled dots. **(D, F)** The bar plots show the mean expression levels of selected genes (TMM-normalized counts) in p53 signaling pathway for HDMB03 (D) and in TNF α signaling pathways for DAOY (F) at different treatment conditions, \pm SD of $n=3$.

Figure 6 – Inhibition of DNA repair enzymes recruitment by AsiDNA favors necrotic cytotoxicity.

(A) Mean percentage of apoptotic and necrotic cells were measured by annexin V/ Propidium iodide staining and analyzed by FACS. Data is represented by the mean \pm standard deviation of $n=3$. **(B, C)** Analysis of the 53BP1 (B) and BRCA1(C) foci formation in HDMB03 cells 2 h after 6 Gy irradiation, with or without 7 μ M AsiDNA treatments. Upper panels: representative images from cells' nucleus; Lower panels: quantification of foci number per nucleus (bar: mean value \pm SEM). NT – non treated conditions. Significance tested by unpaired t-test: * $p<0.05$; ** $p<0.01$; **** $p<0.0001$. Scale bar = 10 μ m. **(D)** Mean percentage of nucleus containing micronuclei (MN) after 72 h after 1.8 Gy irradiation. Significance given by two-way ANOVA test and represented below bar plots. Significance: non-significant, ns; *** $p<0.001$; **** $p<0.0001$. **(E)** Model of the broad-spectrum of AsiDNA radiosensitization in MB cell lines with different *TP53* status.

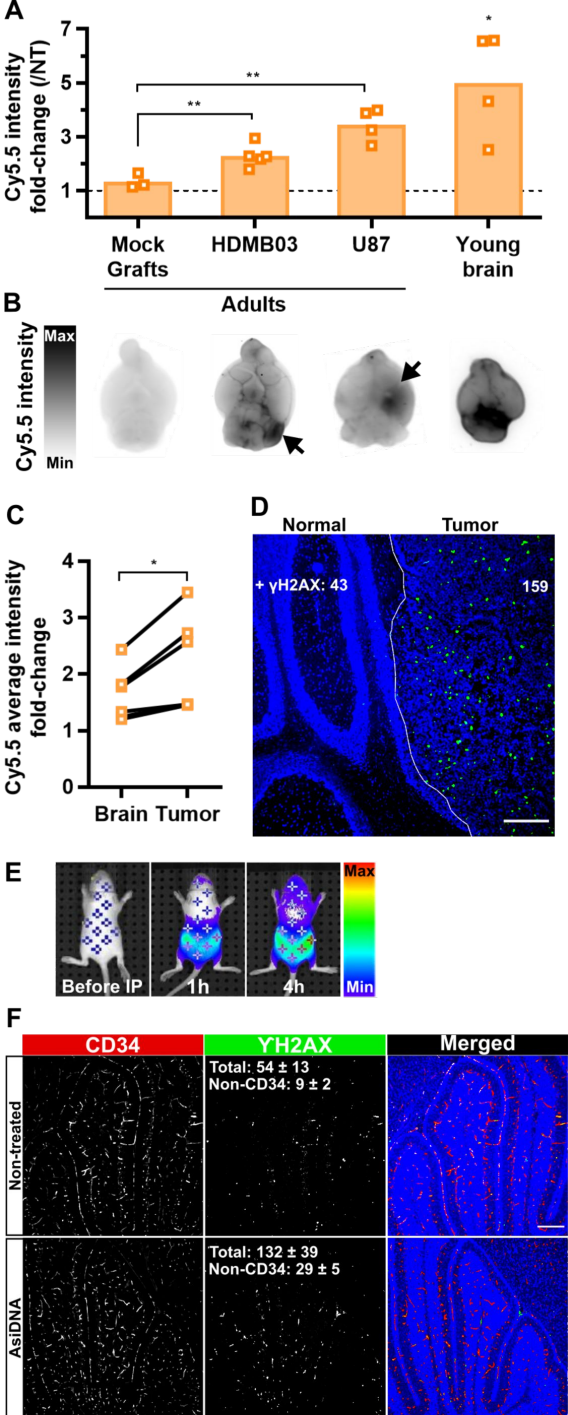


Figure 1

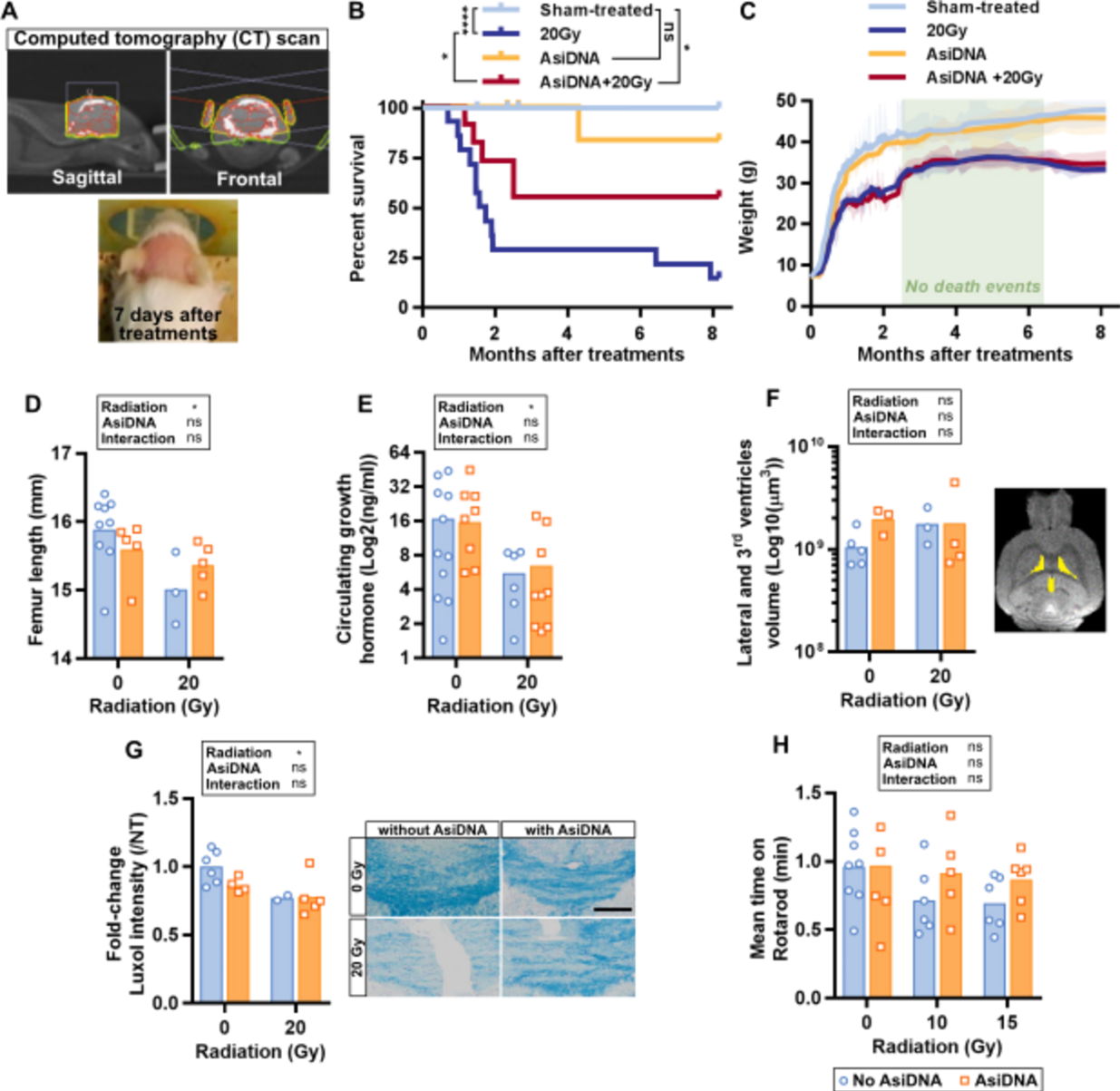


Figure 2

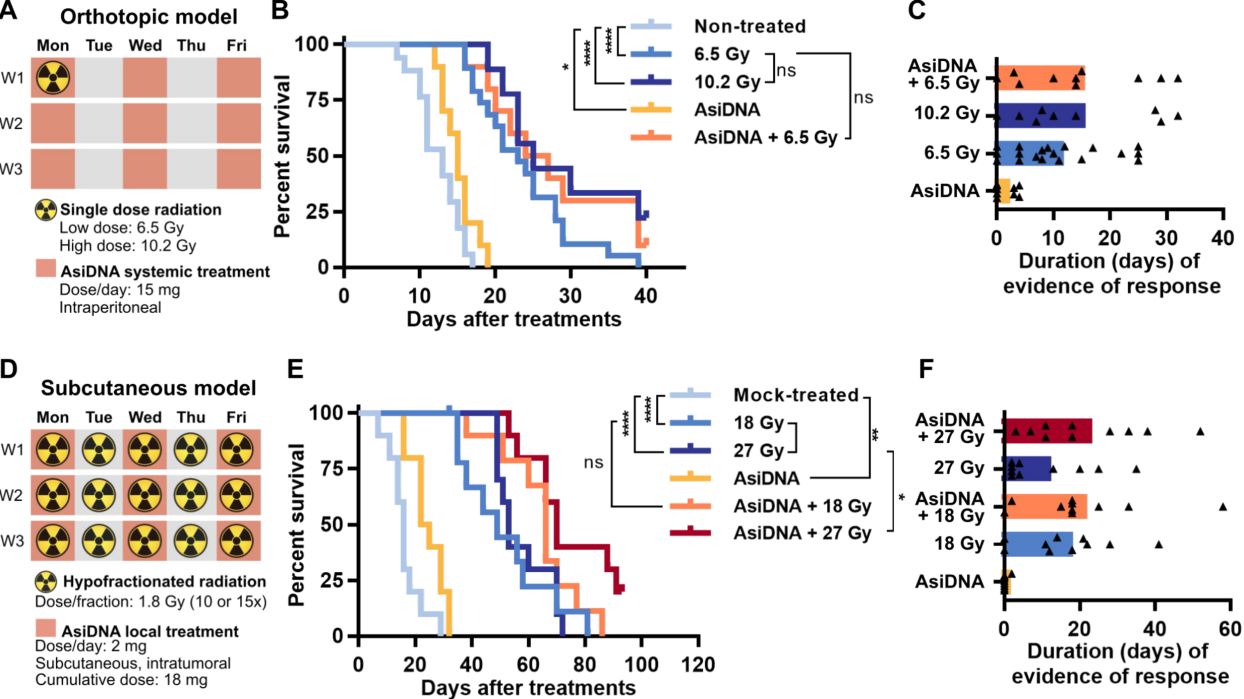


Figure 3

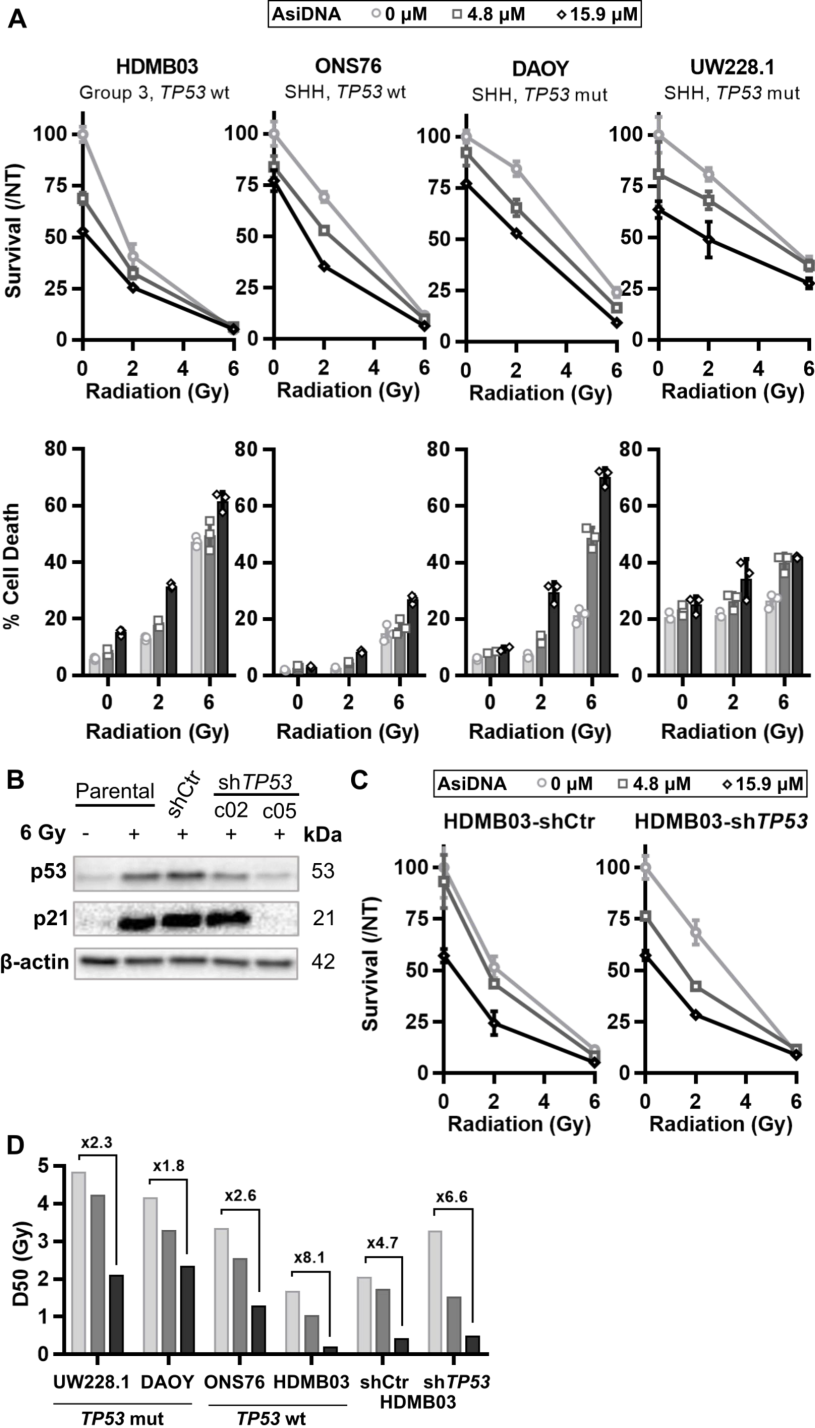


Figure 4

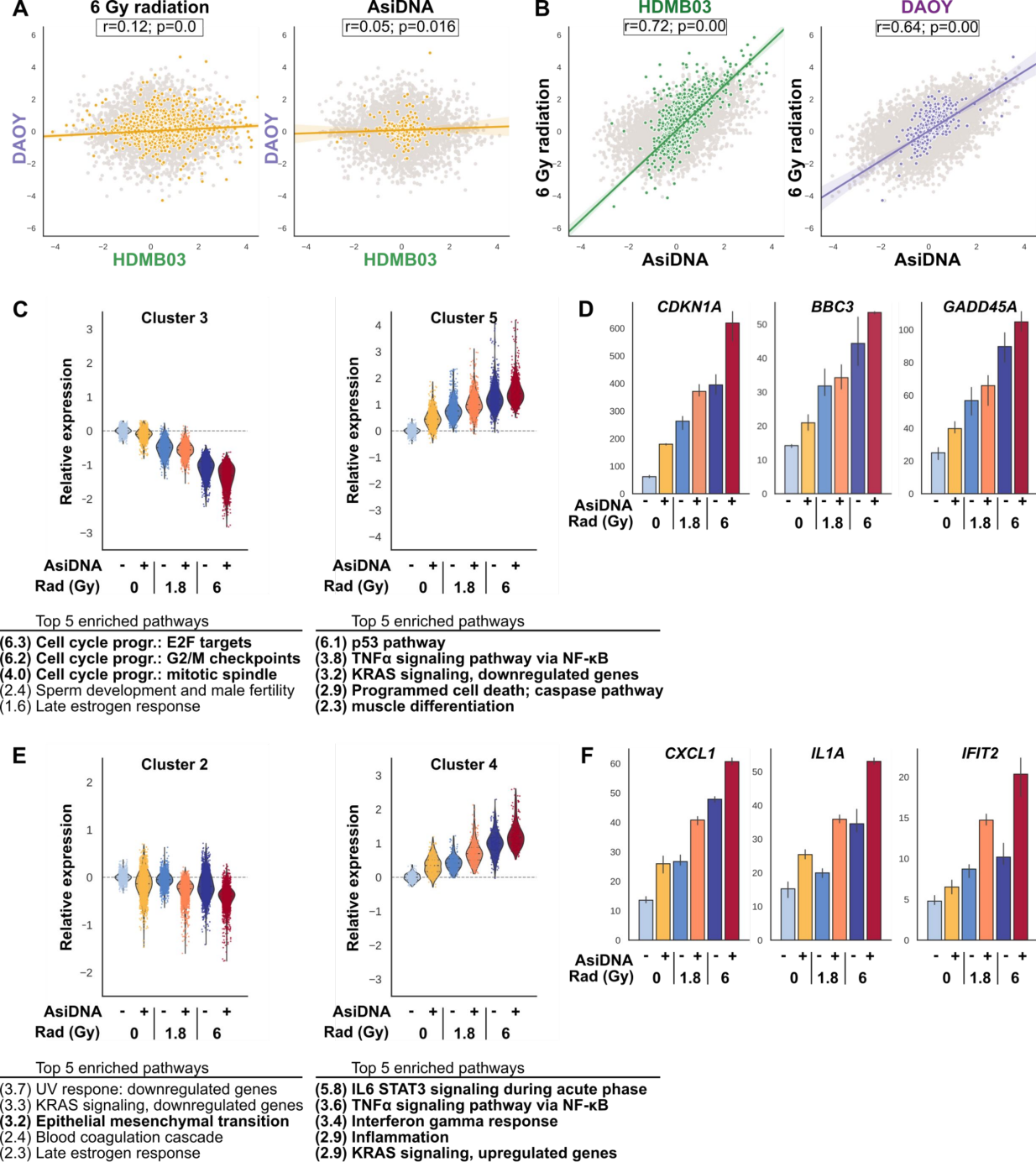


Figure 5

■ Apoptosis ■ Necrosis

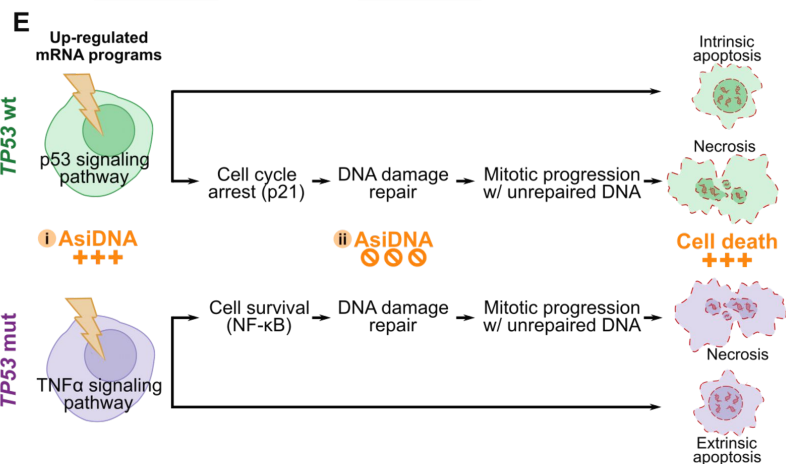
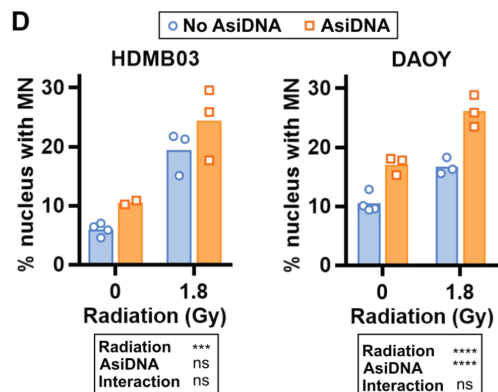
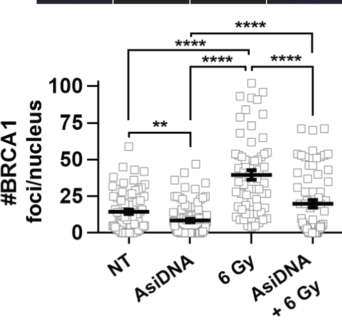
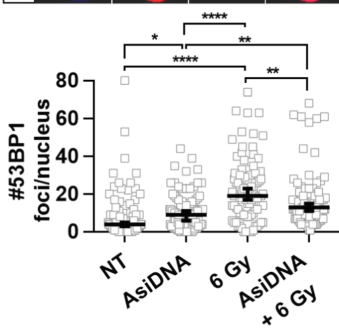
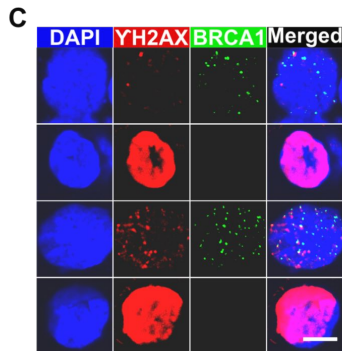
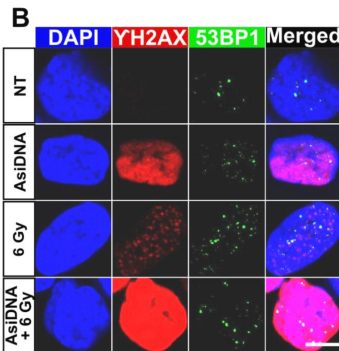
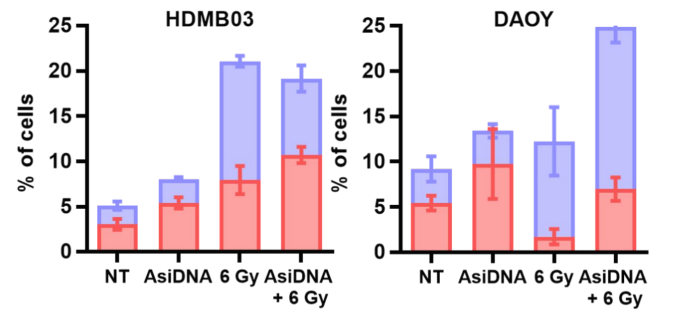


Figure 6